Dalton Transactions

Accepted Manuscript

ROYAL SOCIETY OF CHEMISTRY

www.rsc.org/dalton

Multifunctional pure and Eu^{3+} doped β-Ag_2MoO_4 - Photoluminescence, Energy Transfer Dynamics and Defect induced properties

Santosh K. Gupta[a]*, P.S. Ghosh[b], K. Sudarshan[a], Ruma Gupta[c], P.K. Pujari[a], R.M. Kadam[a]

a. Radiochemistry Division, Bhabha Atomic Research Centre, Mumbai-400085, India

b. Materials Science Division, Bhabha Atomic Research Centre, Mumbai-400085, India

c. Fuel Chemistry Division, Bhabha Atomic Research Centre, Mumbai-400085, India

*Corresponding Author- santufrnd@gmail.com, santoshg@barc.gov.in

Telephone- +91-22-25590636

Fax- +91-22-25505151

Abstract:

Pure and Eu^{3+} doped β-Ag_2MoO_4 was synthesized using co-precipitation method at room temperature. The as prepared compounds were characterized systematically using X-ray diffraction (XRD), photoluminescence (PL) spectroscopy, cyclic voltammetry (CV) and positron annihilation lifetime spectroscopy (PALS). It is observed that pure β-Ag_2MoO_4 gives blue (445 nm) and green (550 nm) emission when irradiated with UV light. The origin of green band was qualitatively explained from density function theory (DFT) calculations using suitable distortion model. It was observed that on doping europium ion, efficient energy transfer from molybdate to europium take place. Excitation spectrum depicting f-f transitions (particularly 395 nm and 465 nm peak) is much more intense than CTB showing that Eu^{3+} ion can be effectively excited by near UV-light. Based on DFT calculations it is proposed that occurrence of Eu^{3+} d-states with conduction band (CB) as well as strong contribution of Eu^{3+} d-states to the impurity level present in the vicinity of the Fermi level, the host (β-Ag_2MoO_4) to dopant (Eu^{3+}) energy transfer is preferable. β-Ag_2MoO_4 *is also explored as a potential candidate for electro catalysis of oxygen reduction reaction (ORR). It was observed that the doping of europium ion in* β-Ag_2MoO_4 *enhances the electrocatalytic activity toward ORR. The presence of large concentration of cation vacancies and large surface defects as suggested by positron annihilation lifetime spectroscopy (PALS) seem to be aiding the ORR.*

1.0. Introductions:

Molybdenum oxides are explored for various applications such as luminescence host, electrochemical devices, sensor, catalyst etc. due to its unique physico-chemical properties **[1]**. Recently it has been found that metal centres such as Ag, Au, Ce, Li or Zr incorporated Molybdenum oxides shows enhanced optical, catalytic, sensing etc. properties compared to pure molybdenum oxide **[2-4]**. In this context silver molybdate has been explored in great detail because of its applications in electrocatalysis **[5]**, photocatalysis **[6, 7]**, optoelectronic devices **[8]**, high temperature lubrication **[9]**, low temperature co-fired microwave devices **[10]**, tribological **[11]**, and optical materials **[12]**.

The host materials play an important role in exploring novel optical materials. Molybdate based inorganic compounds are found to be excellent luminescence hosts due to their unique

crystal structure, high thermal and chemical stability, and ease of synthesis **[13]**. Although lot of reports exist on lanthanide doped metal molybdates **[13-20]**, there is complete scarcity of literature on exploration silver molybdate as luminescence host. Lin *et al.* **[21]** have studied photoluminescence (PL) of europium in Ag_2MoO_4. In this work only excitation and emission spectroscopy of europium doped Ag_2MoO_4 as a function of pH is carried out.

Ag_2MoO_4 exists in two forms α- Ag_2MoO_4 having tetragonal structure and β-Ag_2MoO_4 having cubic spinel structure (A_2BO_4 type) **[22]**.

As far as luminescence of undoped silver molybdate is concerned; Gouveia *et al.***[12]** have observed room temperature visible emission in β-Ag_2MoO_4 which they have attributed to charge-transfer mechanism involving tetrahedral [MoO_4] clusters. They have neither reported excitation spectra nor luminescence lifetime of Ag_2MoO_4.

In most of the reported literature; Ag_2MoO_4 is synthesized by high temperature solid state diffusion method **[7, 10,** and **23]**. Other than solid state route; melt quenching and Czochralski crystal growth method are also used for synthesis of Ag_2MoO_4 **[24, 25]**. But these methods, other than the requiring very high thermal energy, lead to low quality powders with large grain size, irregular morphology etc. Such phosphor powders suffer the problem of poor adhesion in polymer films and glasses which restricts their industrial applicability. On the other hands wet chemical methods like sol-gel, combustion, hydrothermal, reverse micellar, polyol, co-precipitation, polymerization etc score over other techniques as they require low thermal energy and lead to very fine, highly monodisperse and regular sized powder. Hydrothermal methods are extensively used for synthesis of silver molybdate **[12, 26, 27]**. It requires a highly sophisticated autoclave and is very time consuming. It also requires some amount of thermal energy. On the other hand co-precipitation method is relatively simple, rapid and requires very cheap chemicals. Besides being simple, it also offers advantages in (i) control of particle size and composition and (iii) possibilities in modifying the particle surface state and overall homogeneity. Although Rao et al. and Ricci et al. have synthesized silver molybdate using co-precipitation method, their method also require heating in steam, bath for longer time (~ 4-5 Hr) and vigorous stirring.

In our case we have simply mixed the solution of silver nitrate and sodium molybdate solution (prepared) in mili pore water and silver molybdate precipitated out instantaneously.

Other than novelty in synthesis of Ag_2MoO_4; we have explored excitation, emission and lifetime spectroscopy of undoped silver molybdate and tried to bring out the origin of multicolor PL in undoped sample.

Based on energy level diagram different lanthanides emit in different region which can also be tuned depending upon need and usability. Self activated emission takes place in various materials without doping any activator ion (generally lanthanide) **[28]** and they can efficiently transfer their excitation energy when certain lanthanide or any activator ion is doped **[11]**. Therefore, host to lanthanide ion energy transfer has become an efficient route to enhance the photoluminescence intensity of the dopant ion.

An effort was made to correlate the experimental and theoretical results on host-dopant energy transfer takes place. We have tried to figure out why host to dopant complete energy transfer takes place in silver molybdate using theoretical simulation of experimental data.

We have also explored its applicability of silver molybdite for oxygen reduction reaction which can be an important step towards commercially viable fuel cell devices and metal–air batteries for future energy application without employing costly metal like platinum. The electrocatalytic properties of pure and Eu^{3+} doped is correlated with positron annihilation lifetime spectroscopy (PALS). Study of defect chemistry of silver molybdate phosphor doped with Eu^{3+} has is an important step towards realization of highly efficient red phosphor as well as a good electrocatalyst because of the profound role of defect in these fundamental properties.

Europium is a special lanthanide ion because of its peculiarity to exhibit symmetry sensitive emission and has been explored as structural probe as well as for highly efficient red phosphor **[29-33]**.

As far as europium doped β-Ag_2MoO_4 is concerned there is also no detailed report on time resolved photoluminescence, Judd-Ofelt analysis and other photophysical properties.

2.0. Experimental:

2.1. Synthesis of β- Ag_2MoO_4 microparticles

β- Ag_2MoO_4 microparticles were synthesized using rapid and simple co-precipitation technique. In this method 100 mL each of 1 mmol of $Na_2MoO_4.2H_2O$ (99.6 %, J.T. Baker Chemical Company, Phillipsburg, New Jersey) and 2 mmol of $AgNO_3$ (Analytical reagent, 99.9 %, Chemco Fine chemicals, Mumbai) solutions (prepared in Millipore water) were prepared separately. The two solutions were then mixed slowly at room temperature which resulted in the formation of yellow precipitate instantaneously. Within few minutes; pale yellow color of the precipitate turned white. The precipitate was allowed to settle down. The

two components of the mixture (precipitate and supernate) are separated by decanting. The white precipitate so obtained was washed thoroughly using acetone (2-3 times) and dried at room temperature. For europium doping, 17.5mg of Eu_2O_3 (1.0 mol %) was dissolved in dilute nitric acid and the solution is evaporated to dryness under IR lamp. Then it is dissolved in 10 mL of deionized water. 2mL of this solution is added to $AgNO_3$ solution before mixing with Na_2WO_4 solution. Yield was found to be more than 85%.

2.2. Fabrication of the Electrode for Electrocatalysis Measurement:

Electrode was prepared by adding 10 wt% of graphite carbon to 1mg of catalyst (β-Ag_2MoO_4 and Eu doped β- Ag_2MoO_4) followed by adding 5 wt% of nafion solution as the binder. Sufficient amount of isopropyl alcohol (IPA) was then added to make an ink out of which 10 μL (optimized value) was drop casted over a glassy carbon electrode.

2.3. Characterization of β- Ag_2MoO_4 microparticles

The X-ray powder diffraction patterns were recorded using CuKα radiation in a theta–theta geometry diffractometer (supplied by GNR Analytical Instruments Group, Italy; Model: EXPLORER) equipped with a graphite monochromator positioned in the diffracted beam.

PL measurements were done on an Edinburgh CD-920 unit equipped with M 300 grating monochromators. The data acquisition and analysis were done by F-900 software. A 150 W Xenon flash lamp having variable frequency range of 10–100 Hz was used as the excitation source. For this particular sample all measurements were recorded with a lamp frequency of 100 Hz. Multiple Scans (at least five) were taken to minimize the fluctuations in peak intensity and maximize signal-noise ratio. Fluorescence lifetime measurements are based on well established Time-correlated single-photon counting (TCSPC) technique. Lifetime studies were done in the time range of 20 ms where the frequency of Xe lamp was fixed at 10 Hz. Approximately 25 mg of compound in powder form was mixed with few drops of 4 % collodion solution and the resulting slurry was pasted over a glass plate using spatula. This was dried under room temperature and used for further studies.

Cyclic Voltammetry was performed using CHI 760D electrochemical workstation with a three electrode voltammetric cell having glassy carbon disk (GC) working electrode (area, A = 0.031 cm^2), platinum wire counter electrode and Hg/Hg_2SO_4 reference electrode.

The potentials were quoted with respect to Hg/Hg_2SO_4 reference electrode. The measurements were carried out at scan rate ranging from 0.01- 0.1V/s in 1M KOH solution saturated with oxygen. There were IR compensations and no stirring were used for the experiments. All the measurements were carried out at room temperature (25±1°C).

Positron annihilation life time spectroscopy (PALS) measurements were carried out with a lifetime spectrometer of time resolution 260 ps. The lifetime spectrometer was a fast-fast coincidence system with plastic scintillation detectors. Carrier free ^{22}Na, (15 μCi) deposited and dried between two 8 micron kapton films was used as positron source. The positron source was completely immersed in powder samples to stop all positrons in the sample. Approximately one million counts were recorded in each spectrum. Silicon was used as reference for correcting for the positron annihilations in the source. The computer program, PATFIT-88 was used for the analysis of the spectra.

2.4. Computational Methodology:

All calculations in this study are based on density functional theory (DFT) in conjunction with projector augmented wave (PAW) potentials, which is implemented in the plane wave based Vienna Ab-initio Simulation Package (VASP) **[34, 35]**. The generalized gradient approximation (GGA) parameterized by Perdew-Burke-Ernzerhof (PBE) **[36]** was used as the exchange-correlation functional. The projector augmented wave (PAW) potentials **[37]** were used for the ion-electron interactions including the valence states of Ag (4d, 5s – 11 valence electrons), Mo (4p, 5s, 4d - 14 valence electrons), Eu^{3+} (5p, 6s, 5d - 9 valence electrons) and O (2s, 2p – 6 valence electrons). In our calculations, the Kohn-Sham single particle wave functions were expanded in a plane wave basis with kinetic energy cutoff 500 eV and it shown that the results were well converged at this cut off. For cubic β-Ag_2MoO_4 structure, optimization was carried out with respect to plane wave cut-off energy and k-point meshes to ensure convergence of total energy to within a precision 0.1 meV/atom. The total energy of β-Ag_2MoO_4 were optimized with respect to volume (or lattice parameter and c/a ratio) and atomic positions. The structural relaxations (b/a, c/a ratio and atomic positions) were performed for each structure using the conjugate gradient algorithm until the residual forces and stress in the equilibrium geometry were of the order of 0.005 eV/Å and 0.01GPa, respectively. In order to study Eu^{3+} doped system, an Ag atom (out of 16) in the unit-cell of β-Ag_2MoO_4 containing total 56 atoms was replaced by Eu^{3+} atom. The Brillouin-zone (BZ) integrations were performed on an optimized Monkhorst-Pack **[38]** k-point grid of 12x12x12

for β-Ag_2MoO_4. The final calculation of total electronic energy and density of states (DOS) were performed using the tetrahedron method with Blöchl corrections **[39]**.

3.0. Results and discussion:

3.1. Phase purity: Powder X-ray diffraction (PXRD)

Figure 1a depicts the PXRD pattern of undoped and europium doped room temperature synthesized silver molybdate (SMO). It is quite obvious from the pattern that the silver molybdate sample crystallizes in pure *β*-Ag_2MoO_4, as the pattern perfectly matches the stand pattern corresponding to JCPDS card no. 08-0473. The presence of sharp and well-defined XRD peaks indicates a high degree of structural orderings at long-range as well as crystalline nature of as prepared samples. The fact that that XRD pattern doesn't show any diffraction peak related to Ag_2O or Eu_2O_3 phase, indicates of homogeneous solid solution of Ag_2MoO_4 and Eu^{3+}, which further confirms the occupancy of Eu^{3+} ions in lattice position of silver ion in Ag_2MoO_4. The Energy dispersive X-ray fluorescence spectra **(Figures S1 and S2 ESI#)** didn't show any other major impurity.

Figure 1b shows the crystal structure *β*-Ag_2MoO_4 which is drawn using Fullprof Studio version 2 **[40]**. Silver molybdate belongs to the family of compounds with a formula A_2BO_4. It is reported to have two crystalline forms α and β with tetragonal and spinel type cubic structure respectively. The former converts to beta phase on heating ~ 280 ^oC **[41]**. The highlight is room temperature synthesis of pure *β*-Ag_2MoO_4 phase.

The β phase of Ag_2MoO_4 (β-Ag_2MoO_4) is having spinel-type cubic structure characterized by the space group (Fd-3m) with eight molecular formula per unit cell (*Z*=8). The PAW-PBE calculated equilibrium lattice parameters (a=b=c= 9.4154 Å) and volume (834.67 $Å^3$) are matching well with previous Rietveld refinement **[12]**. In these structures, Ag atoms are coordinated to six O atoms at 2.50 Å forming distorted octahedral [AgO_6] clusters with Oh symmetry group. Mo atoms are coordinated to four O atoms at 1.79 Å forms tetrahedral [MoO_4] clusters with T_d symmetry group. Table 1 also compares PAW-PBE calculated equilibrium atomic positions with previously reported atomic positions by Rietveld refinement **[12]**. PAW-PBE calculated atomic positions are in well agreement with experimentally obtained values.

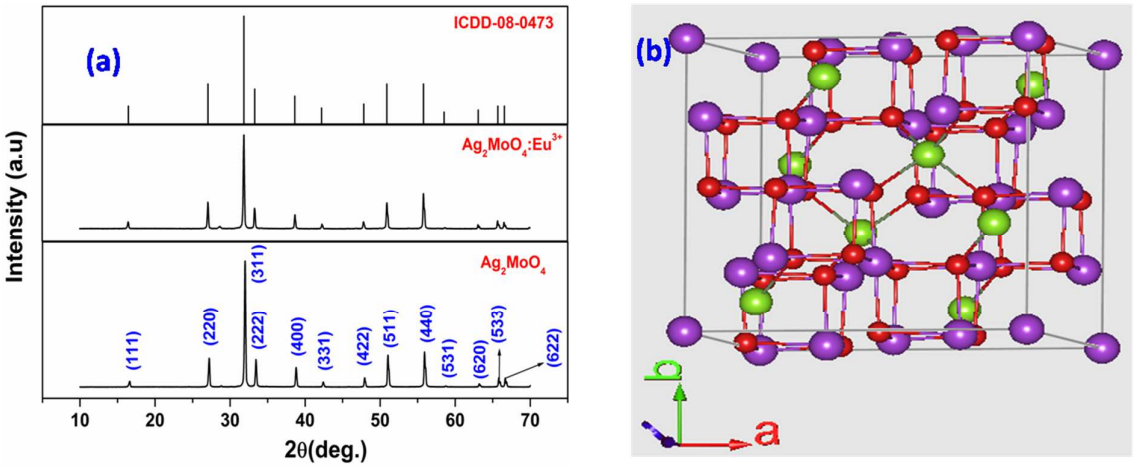

Figure 1: (a) X-ray diffraction pattern of undoped and europium doped silver molybdate. Standard patter corresponding to ICDD No. 080473 is also given. (b) Crystal structure of *β*-Ag_2MoO_4 where purple, green and red ball indicates Ag, Mo and Oxygen atom respectively

Table 1: Lattice parameters, unit cell volume, and atomic positions obtained from DFT based theoretical calculations and experimentally from the structural refinement by the Rietveld Method [12].

Phase	**Lattice parameter (Å)**	**Unit cell volume (Å^3)**	**Bond lengths (Å)**
β-Ag_2MoO_4	a=b=c= 9.4154 a=b=c= 9.317(9) **[12]**	834.67 809.0(1) **[12]**	Ag-O 2.50 ([AgO_6] cluster) Mo-O 1.79 ([MoO_4] cluster)

Atoms	Wyckoff	Theoretical atomic positions			Experimental atomic positions		
		x	*y*	*z*	*x*	*y*	*z*
Ag	*16d*	0.625	0.625	0.625	0.625	0.625	0.625
Mo	*8a*	0	0	0	0	0	0
O	*32e*	0.360	0.360	0.360	0.3524	0.3524	0.3524

3.2. Photoluminescence properties of pure *β*-Ag_2MoO_4

Metal Molybdates are known to exhibit self activated luminescence. They emit in blue –green region and the phenomenon is mostly attributed to charge transfer transition within molybdate moiety. Depending upon the particle size, synthesis condition, thermal treatment, and morphology; this particular visible emission band may vary its position. Such transitions are normally associated with the electron–hole recombination process after excitation using

the band gap of O-Mo charge transfer transition in MoO_4 tetrahedra. In case of silver molybdate; emission spectrum (**Figure 2a**) is displaying two bands at 445 and 550 nm in blue and green region respectively. The peak at 445 nm is attributed to charge transfer transition within distorted MoO_4 tetrahedra **[42]**. Additional green emission peak at 550 nm may arise due to presence of defects/defects clusters. To probe further into origin of defect induced emission at 550 nm; density function theory (DFT) calculations were carried out in pure β-Ag_2MoO_4 which is discussed in the next section 3.3.

To evaluate the colorimetric performance of β-Ag_2MoO_4, CIE chromaticity coordinates were evaluated for undoped sample adopting standard procedures. The values of x and y coordinates of the system were calculated to be 0.290 and 0.315 respectively. This is represented as the point '*' in the CIE diagram shown in **Figure 2b**. It is clear from CIE index values that silver molybdate gives 'near white emission'. This is an important finding considering the cost associated and toxicity of rare earth ion in most of the rare earth based luminescence materials. Considering the importance associated with synthesis of white light material; this can be a small step toward realizing rare earth free white light emitter.

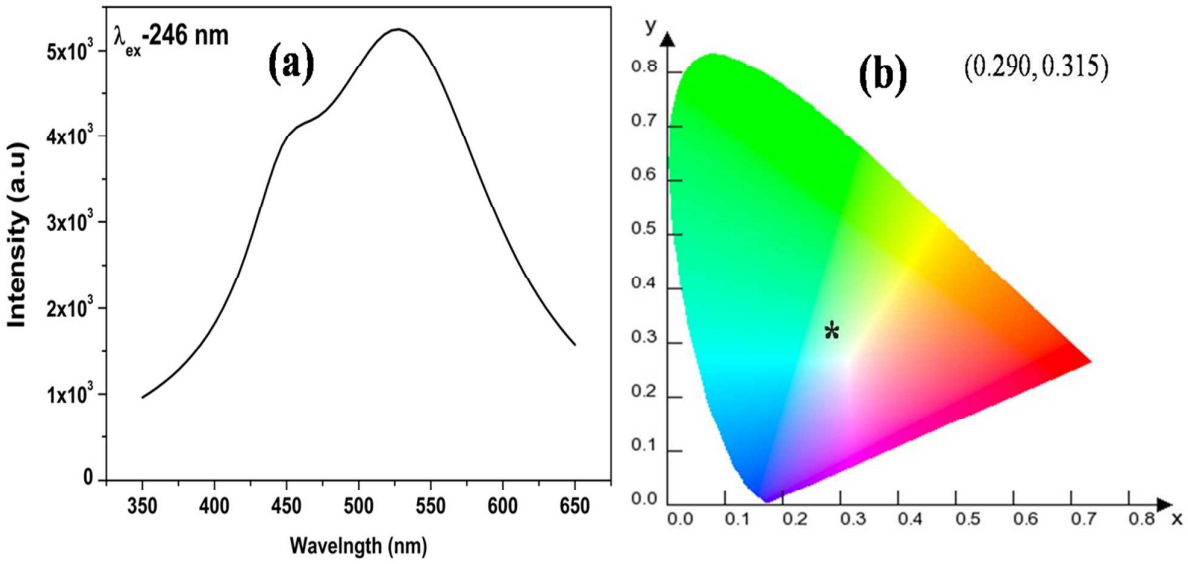

Figure 2: (a) Emission spectrum and (b) CIE index diagram for β-Ag_2MoO_4 microparticles

To get detailed information about the origin of green band in β-Ag_2MoO_4, decay curves were recorded and are shown in **Figure 3**. The PL decay curve was fitted using multi-exponential model using equation:

$$I(t) = A_1 \exp\left(-\frac{t}{\tau_1}\right) + A_2 \exp\left(-\frac{t}{\tau_2}\right) + A_3 \exp\left(-\frac{t}{\tau_3}\right) \quad \textbf{(1)}$$

where I(t) is intensity, τ_1, τ_2 and τ_3 are luminescence lifetime, and A_1, A_2 and A_3 are their relative magnitude. The decay curve shows three different lifetime value 1.36 μs (40 %), 18.14 μs (45 %) and 124.9 μs (15 %). The presence of multiple lifetime lifetimes is an indication for different centres in β-Ag_2MoO_4; which are responsible for its photoluminescence under UV excitation. The lifetime value in the order of 1. 36 μs microseconds is typical of oxygen vacancy related defects **[43]** and is responsible for 550 nm green emission and that in the order of higher value (18 and 125 μs) is lifetime of charge transfer transition in molybdate anion which gives rise to 445 nm peak. The two lifetimes for molybdate transition may arise due to presence of oxygen vacancy in the sample. The average lifetime comes out to be 27.26 μs.

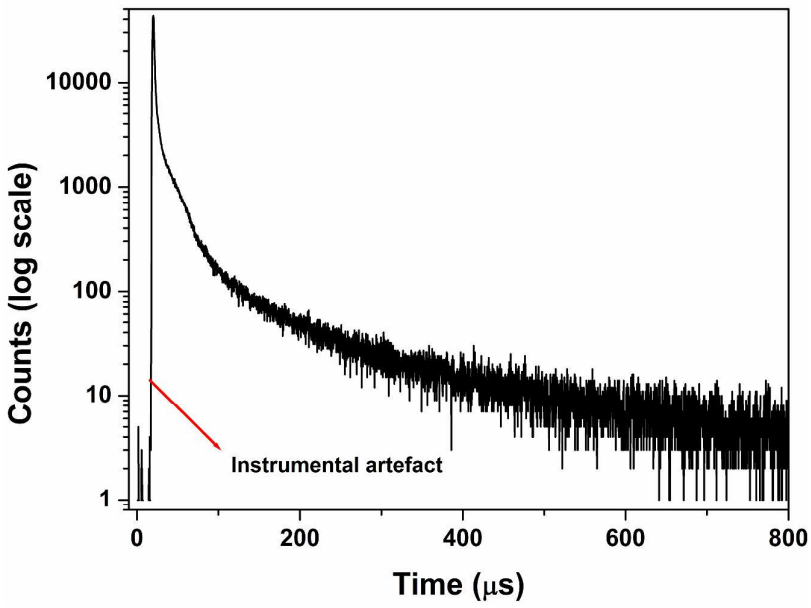

Figure 3: Lifetime decay profile of β- Ag_2MoO_4 microparticles under λ_{ex}-246 nm and λ_{em} 489 nm.

3.3. DFT calculations: the origin of additional peak at 550 nm

In order to simulate order-disorder present in the system as well as structural complex vacancies associated with them three structural models were built: (i) by displacement of Mo atom (β-Ag_2MoO_4_Mo); (ii) by displacement of Ag atom (β-Ag_2MoO_4_Ag) and (iii) by displacement of both Mo and Ag atoms (β-Ag_2MoO_4_Mo/Ag) as described by Gouveia *et al.* **[12]**. The density of states (DOS) were calculated with displacement of 0.25 Å along [001] direction of the unitcell.

The DFT-GGA calculated total and angular momentum projected electronic density of states (DOS) of optimized β-Ag_2MoO_4 and β-Ag_2MoO_4 with Mo atom displaced (β-Ag_2MoO_4_Mo model) are presented in **Figure 4a and 4b,** respectively. **Figure 5a and 5b** shows DFT-GGA

calculated total and angular momentum projected electronic DOS of β-Ag_2MoO_4 with Ag atom displaced (β-Ag_2MoO_4_Ag model) and both Mo/Ag atoms displaced (β-Ag_2MoO_4_Mo/Ag model), respectively. Similar features which can be noted from **Fig. 4 and Fig. 5** is that the lower part of the valence band (VB) from -6 to -4 eV is formed mainly by strong hybridization of the Mo *4d* as well as O *2p* states. Upper part of the valence band from -4 eV to -0.5 eV is composed by strong mixing of Ag *4d* states and O *2p* states. The *d*-states of Mo predominantly and *s*-states of Ag (with small contribution) are present in the conduction band (CB) region. The DFT-GGA calculated electronic band-gap of optimized β-Ag_2MoO_4 is 2.40 eV. Experimentally determined band-gap of β-Ag_2MoO_4 is 3.31 eV **[12]** from UV–visible absorbance spectra (at room temperature) of the β-Ag_2MoO_4 microcrystals processed at 160^{o}C for 1 hour. The DFT-GGA calculated band-gap is underestimated with respect to the experimentally determined values. Such an underestimation of the band gap is well-known for the different exchange-correlation functions of the DFT calculations. But simple GGA reproduces structural properties and insulating nature of β-Ag_2MoO_4 very well.

Displacements of Mo and Mo/Ag atoms in the unitcell of β-Ag_2MoO_4 generate intermediary energy levels in the upper edge of VB and lower edge of CB resulting in reduction of electronic band-gap from 2.40 eV to 2.00 eV. On the other hand, displacement of only Ag atom in the unitcell of β-Ag_2MoO_4 modifies overall DOS but electronic energy-gap remains unaltered. Even though the numerical values of the band-gap of β-Ag_2MoO_4 and distortion models (β-Ag_2MoO_4_Mo, β-Ag_2MoO_4_Ag and β-Ag_2MoO_4_Mo/Ag) are underestimated but our PAW-PBE calculated band-gap values qualitatively reproduces overall trend of previous DFT study using B3LYP hybrid-functional **[12]**. Therefore, the displacement of Mo causes a decreasing of the band gap in comparison to displacements performed on Ag atoms. In this structure, Mo atoms are network former clusters with a strong covalent hybridization between 2p orbitals, which refers to O atoms in VB and 4d orbitals of Mo atoms in the CB. The perturbation in tetrahedral [MoO_4] clusters creates new intermediate levels in the forbidden region, promoting different electronic transitions and decreasing the electronic band-gap. When a defect in the structure (β-Ag_2MoO_4_Mo model) was caused by the atomic displacement of 0.25 Å on the Mo atom, two kinds $[\boldsymbol{MoO_4}]'_{\boldsymbol{o}}$ and $[\boldsymbol{MoO_4}]^{\bullet}_{\boldsymbol{d}}$ of clusters were observed, in which the subscript ' is the cluster with one electron, and • is the cluster with one hole. Therefore, our DFT based calculations show presence of order-disorder phenomena caused by [MoO_4] clusters (represented by β-Ag_2MoO_4_Mo distortion model) which qualitatively explains the host emission of β-Ag_2MoO_4 in green

region (see Fig. 2(a)). In this study, we aim to provide a qualitative explanation of photoluminescence properties of β-Ag_2MoO_4 microcrystals by using a distortion model with DFT calculations. So change in electronic density of state (DOS) features compared to ideal β-Ag_2MoO_4 is important to understand the origin of impurity states in the vicinity of Fermi level and lower part of conduction band. In other words, effects of oxygen vacancy clusters in the photoluminescence properties of β-Ag2MoO4 microcrystals can be explained qualitatively from this DFT calculation even though numerical values of electronic band-gaps are underestimated.

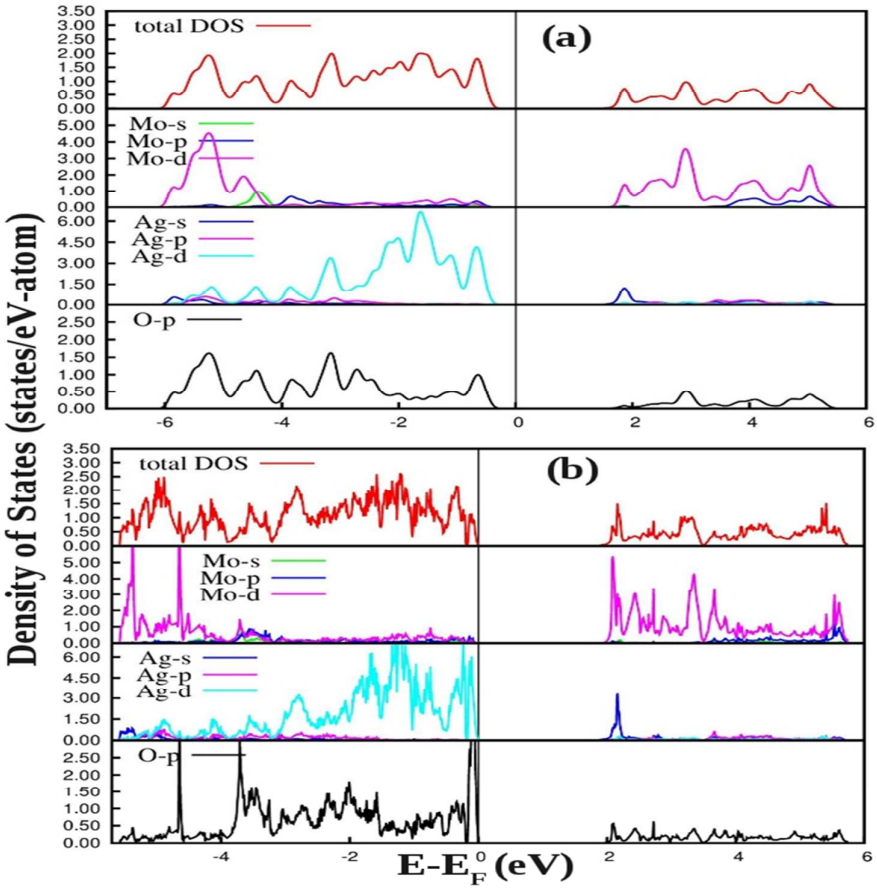

Figure 4: DFT-GGA calculated total and angular momentum decomposed density of states (DOS) of pure β-Ag_2MoO_4 (a) and β-Ag_2MoO_4_Mo distortion model (b). The vertical lines at 0 eV represent Fermi energy (E_F).

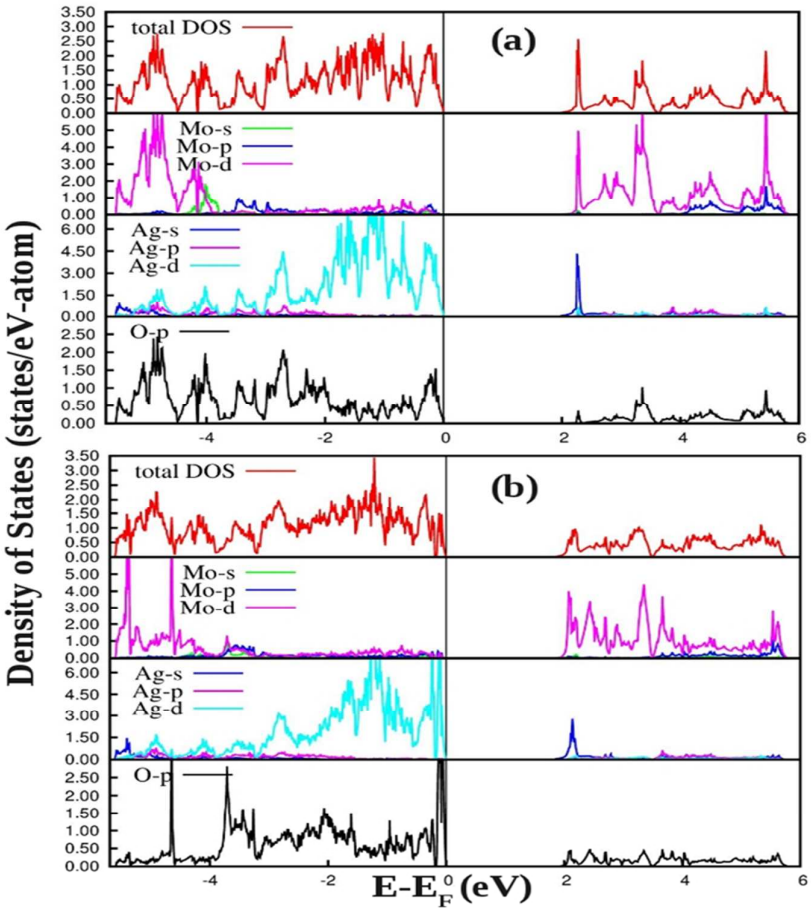

Figure 5: DFT-GGA calculated total and angular momentum decomposed density of states (DOS) of β-Ag_2MoO_4_Ag distortion model (a) and β-Ag_2MoO_4_Mo/Ag distortion model (b). The vertical lines at 0 eV represent Fermi energy (E_F).

3.4. Photoluminescence properties of Europium doped *β*-Ag_2MoO_4

Figure 6 shows the excitation spectra of Eu^{3+}-doped Ag_2MoO_4 sample. Broad band in the region 210–290 can be attributed to charge transfer band (CTB). In general; CTB can arise because of three different mechanisms: (i) host absorption which involves electron transfer from O^{2-} ligand to Mo^{6+} (ii) inter-valence charge transfer due to electronic transition from 4f state of Eu^{3+} to Mo^{6+} and (iii) electron transfer from the filled 2p orbitals of O^{2-} anions to the vacant 4f orbitals of Eu^{3+} **[44]**. Such broadness in CTB can mostly arise through contribution from all the three types of electronic transition.

Highly sharp and intense lines in the region 300-550 nm are attributed to intra-configurational f-f transition of Eu^{3+}. Within these transitions, the ($^7F_0 \rightarrow {}^5L_6$) at 395 nm and ($^7F_0 \rightarrow {}^5D_2$) at 465 nm are the most intense ones and the less intense peaks were observed at 361 nm ($^7F_0 \rightarrow {}^5D_4$), 380 nm ($^7F_0 \rightarrow {}^5G_2$, $^5G_3$), 414 nm ($^7F_0 \rightarrow {}^5D_3$), and 533 nm ($^7F_0 \rightarrow {}^5D_1$). This indicates that the ultra-violet (UV), near-UV, UV B (UVB), and blue laser diodes/LEDs

can act as effective pumping sources for the red emission from Eu^{3+} ions. Normally the excitation spectrum of Eu^{3+} ion consists of only relatively narrow and weak f–f transition from 300 to 550 nm because they are forbidden in nature compared to allowed charge transfer transition in the region 220-280 nm. Therefore, Eu^{3+} ion cannot be efficiently excited by near UV light. To overcome these drawbacks, proper sensitizer ions or hosts materials must be selected to sensitize Eu^{3+} to obtain ideal luminescent materials. But in this particular host; f-f transition (particularly 395 nm and 465 nm peak) is much more intense than CTB; therefore Eu^{3+} ion can be effectively excited by near UV-light.

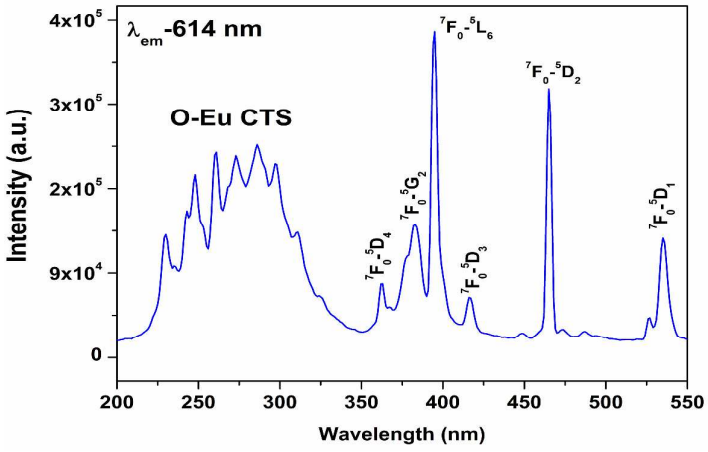

Figure 6: Excitation spectrum of Ag_2MoO_4: Eu (λ_{em}-614m nm)

Upon excitation at 260 nm (Charge transfer band), the emission spectrum shown in **Figure 7a** exclusively contains very strong bands of $^5D_0 \rightarrow {}^7F_1$ (592 nm), $^5D_0 \rightarrow {}^7F_2$ (614 nm), $^5D_0 \rightarrow {}^7F_3$ (653 nm) and $^5D_0 \rightarrow {}^7F_4$ (704 nm). Compared with the emission peaks of Eu^{3+}, the intrinsic blue-green emission from MoO_4^{2-} groups is very weak, suggesting the existence of efficient energy transfer from MoO_4^{2-} cluster to doped Eu^{3+} ion in Ag_2MoO_4: Eu.

The emission spectrum shows characteristics emission lines of Eu^{3+} involving ($^5D_0$-^7F_j, J=0-4). It is well known that $^5D_0 \rightarrow {}^7F_1$ emission of Eu^{3+} ion at 593 nm is magnetically allowed and is referred as magnetic dipole transition (MDT) and it is not affected much or invariably unaffected by local environment around the Eu^{3+} ion, whereas the $^5D_0 \rightarrow {}^7F_2$ Eu^{3+} ion at 615 nm is electrically allowed and referred as electric dipole transition (EDT) is an extremely sensitive transition to local environmental factor such as symmetry and local field in the vicinity of the Eu^{3+} ion. Because of this peculiar characteristic; $^5D_0 \rightarrow {}^7F_2$ transition of Eu^{3+} is also termed as hypersensitive electric dipole transition. The integral ratio of EDT and MDT emission intensity; which as known as asymmetry factor gives an idea about the extent of local structural distortion when $Eu^{(III)}$ is doped in any inorganic host.

The fact that in Ag_2MoO_4; $^5D_0$-$^7F_2$ transition at 614 nm (EDT) is much more intense than the $^5D_0 \rightarrow {}^7F_1$ transition at 593 nm (MDT); indicates that Eu^{3+} at Ag site deviates from inversion symmetry and the local symmetry around europium ion in Ag_2MoO_4 is quiet low.

In most of the europium based luminescence materials; on using excitation wavelength of ~390-400 nm; the intensities of emission bands are relatively very weak compared to that obtained on excitation with charge transfer band (CTB). This is because of the fact; that Eu^{3+} absorption bands corresponding to the f-f transitions are La-Porte forbidden and exhibit extremely poor absorptivities in UV region and hence the relatively emission intensity is very weak.

But requirement of high efficiency and low power consuming red emitting phosphor required it to be excitable under near UV (~395 nm) or blue light (~465 nm). From **Figure 7b**; it can be very well seen that Ag_2MoO_4: Eu can be easily excited using 395 and 465 nm giving an intense red $^5D_0 \rightarrow {}^7F_2$ emission at 615 nm.

Eu^{3+}-doped red phosphors has gained much importance in the area of phosphor converted white-light emitting diodes (w-LED[s]) because they exhibit a high lumen equivalent, quantum yield and are quiet photostabe **[45]**.

To evaluate the material performance on color luminescent emission, CIE chromaticity coordinates were evaluated for Ag_2MoO_4: Eu phosphor under excitation wavelength of 395 and 465 nm corresponding to $^7F_0 \rightarrow {}^5L_6$ and $^7F_0 \rightarrow {}^5D_2$ transition of Eu^{3+} ion adopting standard protocol. It can be clearly seen from the diagram and the calculated values, that Ag_2MoO_4: Eu sample give an in intense red emission due to presence of relatively intense 614 nm lines ($^5D_0 \rightarrow {}^7F_2$) under both 395 and 465 nm excitation. This is represented as the point '*' and '#in the CIE diagram shown in **Figure 7c.**

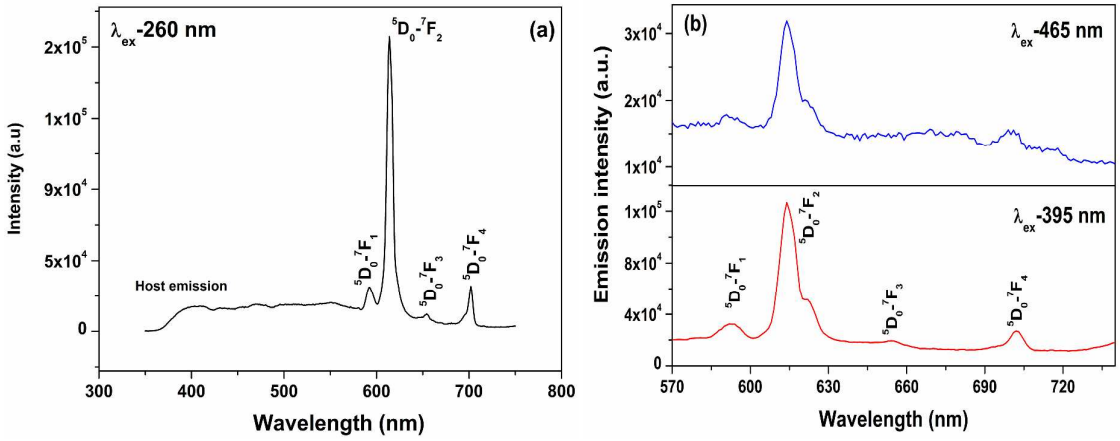

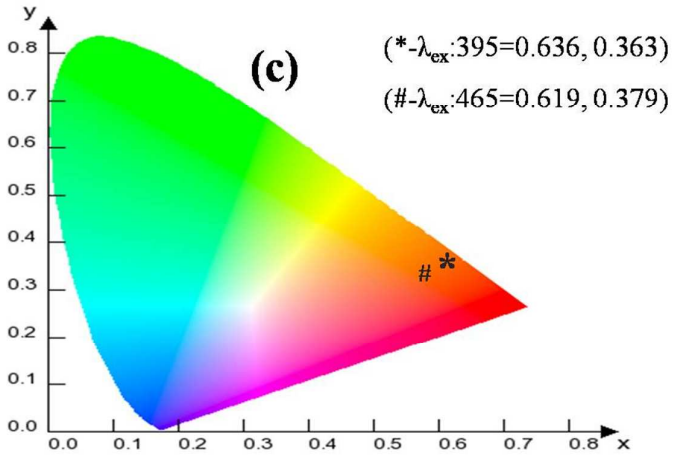

Figure 7: (a) Emission spectrum of Ag_2MoO_4: Eu (a) under excitation by charge transfer state (260 nm) (b) under near UV excitation (395 and 465 nm) and (c) CIE diagram showing the co-ordinates and representing the color emitted by Ag_2MoO_4: Eu on 395 and 465 nm excitation

3.5. Time resolved emission spectroscopy of Europium doped *β*-Ag_2MoO_4

As discussed in the section structural and XRD part that in beta silver molybdate with spinel structure; the coordination number of Ag ion is 6 and that of Mo ion is 4. These are the possible two cationic sites which can be occupied by the Eu^{3+} ions. Based on ionic size consideration it is assumed that Eu^{3+} occupy Ag^{+} sites only because the ionic radii of 0.947 Å for Eu^{3+} is slightly smaller than that of 1.15 Å for Ag^{+}, on the other hand its is much larger than that of 0.41 Å for Mo^{6+} in 4-fold coordination. But the difference in charges between Eu^{3+} and Ag^{+} would result in the deviation of the site symmetry of Eu^{3+} from O_h symmetry (AgO_6 in Ag_2MoO_4) due to the charge compensation effects resulting in intense EDT.

To get an idea about such site occupancy by europium ion in Ag_2MoO_4: Eu we have conducted luminescence life time decay measurements. The decay curves corresponding to the $^5D_0$ level of Eu^{3+} ions in the 1.0 mol % Eu^{3+} doped Ag_2MoO_4 are shown in **Figure 8** under excitation wavelength of 260 nm and emission wavelength of 614 nm. For Ag_2MoO_4: Eu, decay curve obeys a biexponential behavior and the fitted equation is mentioned in equation (1). The decay curve shows two different lifetime value 75.8 µs (T1) and 298.5 µs (T2) with magnitudes 25 and 75 % respectively with average lifetime of 282.5 µs.

It is puzzling that although europium is occupying only silver site; still decay is following biexponential behavior.

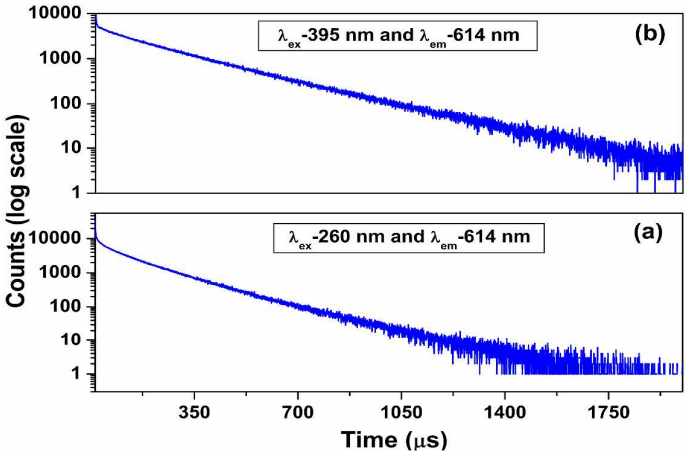

Figure 8: Luminescence decay profile of $^5D_0$ level of europium in Ag_2MoO_4: Eu (a) under 260 nm and (b) 395 nm excitation

In order to identify the local environment associated with the species exhibiting different life-times (~ 76 and 300 μs), time resolved emission spectra (TRES) were recorded at different time-delays (50 and 350 μs) with constant integration time of 40μs. The spectrum obtained after 350 μs delay is expected from long-lived europium ion (300 μs) as the short species would have reduced in intensity by a factor of e^{-5}. The spectra obtained after 50 μs delay time has contributions from both short-lived (T_1) and long-lived species (T_2). The spectral characteristics of short lived species were obtained by subtracting the contribution of long-lived species (obtained mathematically using the spectra observed after 350 μs delay) from the observed spectra of 50 μs delay. Spectra for short lived and long lived species obtained after mathematical calculations are shown in the **Figure 9**. The asymmetry ratio was found to be 7.45 and 5.23 for short lived (τ= 76 μs) and long lived (τ= 300 μs) europium ion respectively. This is in correspondence with phonon energy concept where short lived species will have more asymmetric component than long lived species.

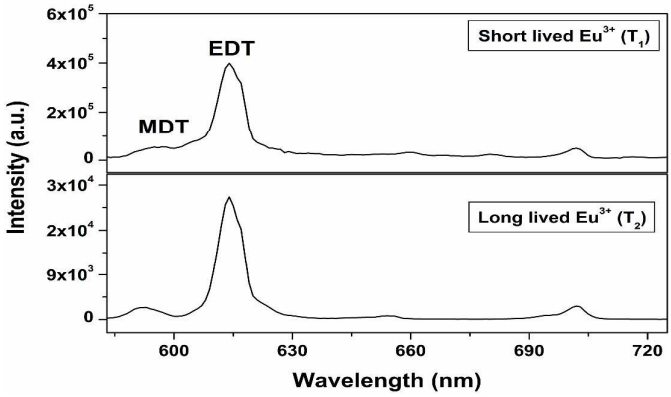

Figure 9: Time-resolved emission spectra of for short and long lived Eu^{3+} ion in Ag_2MoO_4

3.6. MoO_4^{2-} to the Eu^{3+} energy transfer

It is reported that in solid-state luminescent materials where possibility of energy transfer process exists, when the host materials or sensitizers are excited (indirect excitation), some luminescence decay curves from the rare-earth activator could follow a non-exponential function **[46, 47]**. As discussed that for $Ag_2MoO_4:Eu^{3+}$ phosphor, there exists significant amount of energy transfer from MoO_4^{2-} anionic complex to Eu^{3+} excitation at 260 nm, and this is followed by the luminescence decay from the $^5D_0$ level of Eu^{3+} .

The energy transfer from MoO_4^{2-} moiety to the Eu^{3+} in $Ag_2MoO_4:Eu^{3+}$ can be used to change the relative intensity of blue-green emission (MoO_4^{2-}) and red emission (Eu^{3+}), and hence multi-color luminescence is realized. Other interesting things which we have observed is that on excitation with 395 nm, luminescence decay profile shows single lifetime only and can be fitted into a single exponential function:

$$\mathbf{I(t) = Aexp\ (-t/\tau)} \qquad \mathbf{(2)}$$

This indicates that on exciting with intra f-f transition of europium ion; no energy transfer takes place from host to europium ion; which also get's reflected in lower lifetime value of Eu^{3+} compared to energy transfer assisted process on 260 nm excitation. These results are in consistence with previous reports **[47]**.

It is interesting that average lifetime value of Ag_2MoO_4 in $Ag_2MoO_4:Eu^{3+}$ doped sample (14 .59 μs) is smaller than undoped sample (27.26 μs) under similar condition of λ_{ex} and λ_{em}. This also leads to conclusion that energy transfer has indeed taken place from molybdate ion to europium in doped sample leading to reduction in its lifetime.

The energy transfer efficiency (η) and energy transfer rate (ω_{ET}) from Ag_2MoO_4 to Eu^{3+} can be calculated by the following equation 3 and 4 **[48, 49]**:

$$\eta = 1-\tau/\tau_0 \qquad (3)$$

$$\omega_{ET} = 1/\tau - 1/\tau_0 \qquad (4)$$

Where τ_0 and τ represent the lifetime of host in the absence and presence of Eu^{3+}, respectively. The value of η and ω_{ET} calculated in this case is 46.47 % and 3.23×10^3 s^{-1}.The mechanism of energy transfer from molybdate to europium trivalent ion is pictorially depicted in **Figure 10**.

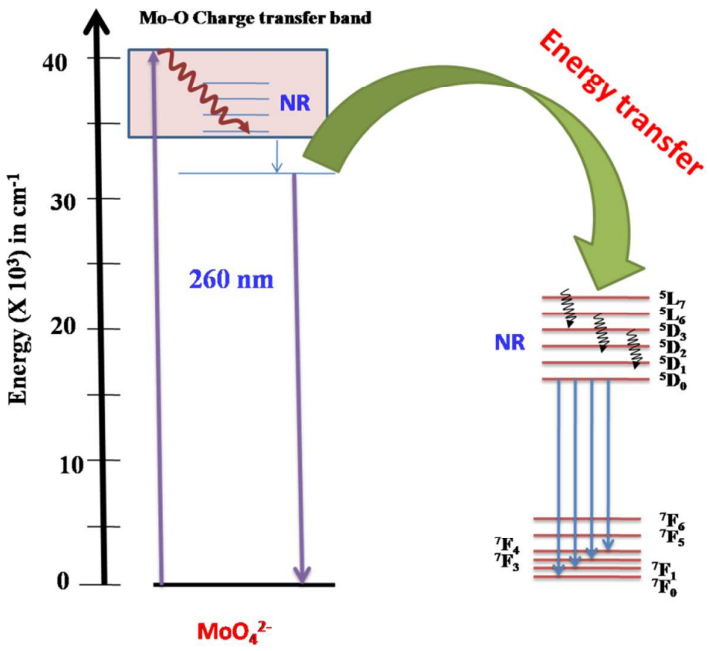

Figure 10: Energy level scheme for the Eu^{3+} and MoO_4^{2-} group and the energy transfer mechanism from MoO_4^{2-} to Eu^{3+}.

In order to understand nature of chemical interactions and feasibility of energy transfer between host β-Ag_2MoO_4 matrix and Eu^{3+} dopant we calculated electronic DOS of Eu^{3+} doped in β-Ag_2MoO_4_Mo distortion model by DFT and shown in **Figure 11**. Overall bonding features are same for β-Ag_2MoO_4 _Mo and Eu^{3+} doped β-Ag_2MoO_4 _Mo but some notable differences are present. Due to Eu^{3+} doping Fermi energy has shifted to bottom of the CB and an appreciable amount of impurity states are present at the Fermi level and in the vicinity of the Fermi level. These impurity states are composed of Eu^{3+} *d*-states majorly and Mo *d*-states. Presence of impurity states at the vicinity of CB minimum further reduces DFT-GGA calculated electronic band-gap of Eu^{3+} doped β-Ag_2MoO_4 _Mo which is 1.80 eV. It can also be noted from **Figure 11** that Eu^{3+} *d*-states are localized of in the whole CB of β-Ag_2MoO_4 majorly. Therefore, coincidence of Eu^{3+} *d*-states with CB as well as strong contribution of Eu^{3+} *d*-states in the impurity levels present in the vicinity of the Fermi energy

predicts host (β-Ag_2MoO_4) to dopant (Eu^{3+}) energy transfer is easy and preferable.

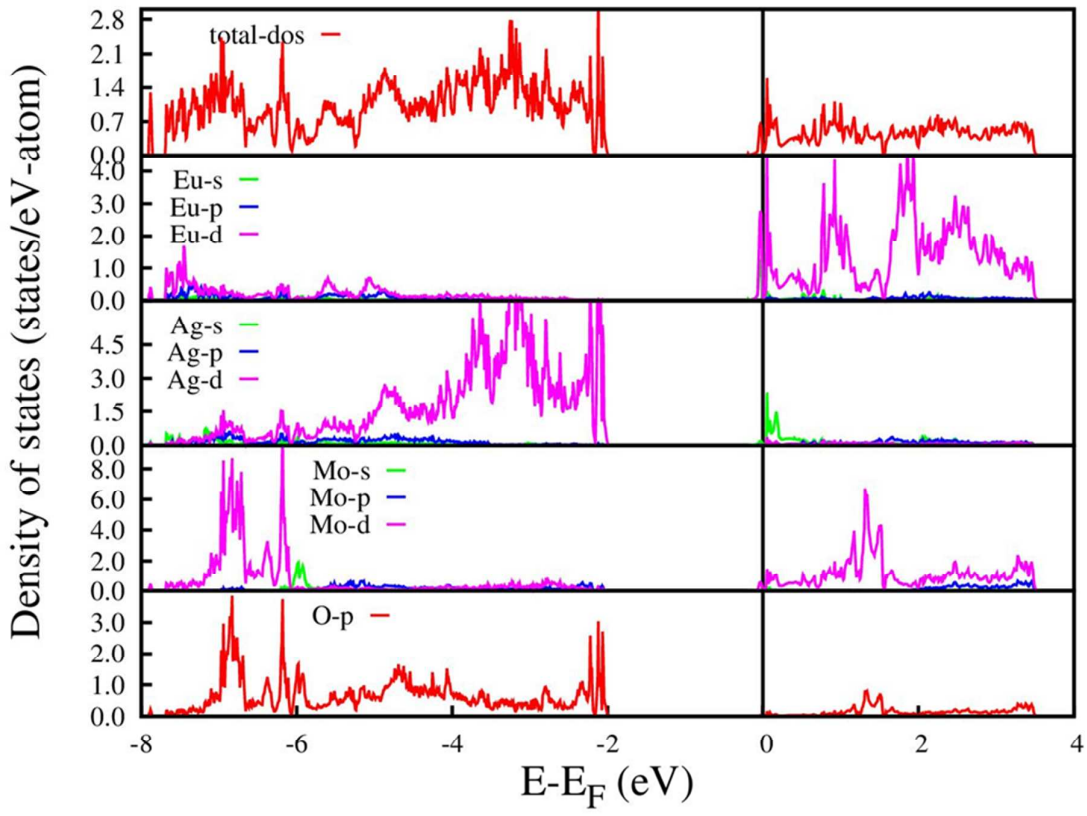

Figure 11: DFT-GGA calculated total and angular momentum decomposed density of states (DOS) of β-Ag_2MoO_4_Ag distortion model with Eu^{3+} doping in place of Ag. The vertical lines at 0 eV represent Fermi energy (E_F).

3.7. Judd-ofelt analysis of Eu^{3+} ion doped Ag_2MoO_4

Judd-ofelt analysis is a very powerful tool for evaluating photophysical properties of europium ion in doped sample using the corrected emission spectrum. The details of all the calculations used are explained extensively elsewhere **[44, 50]**. For all the calculation corrected spectra corresponding to 395 nm excitation wavelength is used.

The value of refractive index used for Ag_2MoO_4 is 2.446 calculated using Gladstone Dale equations

$$\frac{n-1}{\rho} = k1\frac{p1}{100} + k2\ \frac{p2}{100}(5) \qquad \textbf{(5)}$$

Where k = Gladstone-Dale constant (n-1/ρ) of chemical species i, p= percentage of chemical species i.e. Ag_2MoO_4 consists of 50 % Ag_2O and 50 % % MoO_3. Data used in the calculation of refractive index for Ag_2MoO_4 is mentioned in **Table 2**. Density of Ag_2MoO_4 used is 6.18 g/cc.

Table 2: Data used in calculation of refractive index for silver molybdate

	Density (g/cc)	Refractive index of constituent
Ag_2O	7.14	2.50
MoO_3	4.69	2.21

It is well known that the parameter Ω_2, is an indication of the dominant covalent nature and/or structural changes in the vicinity of the Eu^{3+} ion (short range effects), while Ω_4 intensity parameters are long range parameters that can be related to the bulk properties such as viscosity and rigidity of the inorganic matrices. The Ω_2 parameter is related to the degree of covalence and polarizability of the chemical environment experienced by the Eu^{3+} ion; higher Ω_2 values point to more covalent and polarizable environments. In case of Ag_2MoO_4: Eu; Ω_2 value was found to be greater than Ω_4 indicating high covalency and low symmetry around europium ion which is also observed in emission spectrum where EDT dominate MDT. This is well in agreement with high asymmetry value of Eu^{3+} in Ag_2MoO_4. The calculated τ_R for the excited $^5D_0$ level of Eu^{3+} ion is found to be 542 μs, which is larger than the τ_{exp} (250 μs). This difference in τ_{exp} and τ_{cal} can be attributed to nonradiative decays. There are lots of factor which contributes to non-radiative transition such as presence of defects, low vibrating oscillator, surface inhomogeneity etc. The trend in branching ratio-suggests most of radiative energy goes in the $^5D_0 \rightarrow {}^7F_2$ transition. This is also observed from emission spectrum where $^5D_0 \rightarrow {}^7F_2$ transition is much more intense than $^5D_0$-$^7F_1$. The Judd-Ofelt parameter and other properties calculated for Eu^{3+} in Ag_2MoO_4 is mentioned in **Table 3**. The quantum efficiency of this particular phosphor which is defined as the ratio of the experimental lifetime to the calculated radiative lifetime of the $^5D_0$ level is around 46.2 %.

Table 3: J-O intensity parameters and radiative properties for Eu^{3+} in Ag_2MoO_4

Transition	A_{Red} (s^{-1})	A_{Rmd} (s^{-1})	Ω_J (10^{-20} cm^2)	β_J (%)	η (%)	A_R (s^{-1})	A_{NR} (s^{-1})
$^5D_0 \rightarrow {}^7F_1$	0	211	-	11.4	46.2	1850	2155
$^5D_0 \rightarrow {}^7F_2$	1120	0	6.47	60.6			
$^5D_0 \rightarrow {}^7F_4$	516	0	6.20	28.0			

3.8. Electrocatalytic property toward oxygen reduction reaction (ORR) of pure and Eu^{3+} doped Ag_2MoO_4

To explore the potential applications of undoped and Eu^{3+} doped Ag_2MoO_4 as electro-catalysts toward oxygen reduction reaction (ORR), cyclic voltammetry (CV) was performed. **Figure 12a** shows the cyclic voltammogram of Ag_2MoO_4 (1) in oxygen saturated 1 M KOH at a scan rate of $0.01Vs^{-1.}$ The cyclic voltammogram of Eu doped Ag_2MoO_4 (1*) is overlaid in the same scale for the sake of comparison. It shows two reduction peaks. Peak (a) at around 0.05 V can be attributed to a two electron reduction process described by equation (6) **[51, 52]**:

$$O_2 + H_2O + 2e^- \rightarrow HO_2^- + OH^- \quad (6)$$

The second broad reduction peak (b) at around -0.3 V can be assigned to a further two electron reduction process described by equation (7):

$$HO_2^- + H_2O + 2e^- \rightarrow 3OH^- \quad (7)$$

The anodic peak at 0.2 V can be assigned to the oxidation of Ag to Ag_2O. It can be clearly seen that when the catalyst is doped with Eu^{3+} ion; although the peak positions are almost similar but the intensity of current is increased drastically. The drastic increase in the current could be due to large number of negatively charged cation vacancies and other oxygen related defects created in the europium doped sample due to size and ionic charge mismatch. The relative changes in the defects between pure and europium doped are discussed in the next section. The defects can provide more active sites for the electrochemical charge transfer to take place thereby increasing the intensity of current. Presence of large oxygen vacancy clusters on the surface would aid the adsorption of oxygen on the surface. The plot of peak current vs scan rate showed a linear behaviour confirming the adsorbtion of O_2 at the catalyst surface during reduction. **Figure 12b** shows the oxygen reduction reaction at bare glassy carbon and bare Platinum surface. The onset potential of ORR at Pt electrode is around -0.1 V and for GC electrode it is -0.3 V. It suggests that the reduction peaks are obtained at more negative potential compared to the one obtained at both doped and undoped catalyst respectively. It confirms that there is a strong interaction between adsorbed oxygen and Ag_2MoO_4. There can be an electronic effect between Ag and MoO_4 facilitating adsorbtion of O_2 leading to O-O bond splitting and increase in the catalytic activity **[53]**.

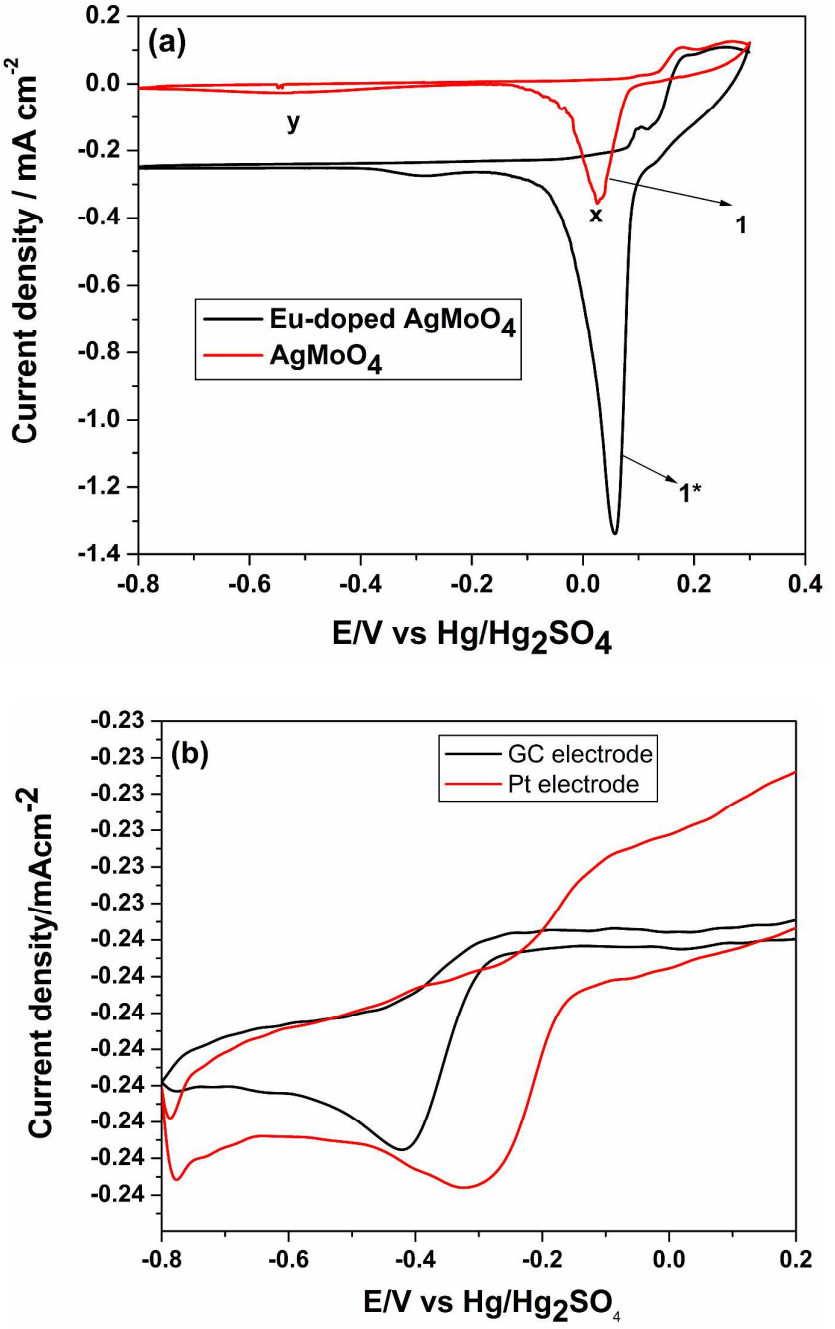

Figure12: Cyclic voltammograms at (a) Ag_2MoO_4 (1) and Eu doped Ag_2MoO_4 (1*) drop casted at glass carbon electrode in oxygen saturated 1 M KOH at a scan rate of 0.01Vs^{-1}. (b) Glassy carbon and Platinum surface in oxygen saturated 1 M KOH at a scan rate of 0.01Vs^{-1}.

3.9. Positron annihilation lifetime spectroscopy

The positron annihilation lifetime spectra could be fitted well with three components. A long lived component of 2.1 ns and 2% intensity was obtained in both undoped and Eu^{3+}

doped Ag_2MoO_4. Though the origin of this component is not very clear, it is reported in many powder samples **[54]**. The other two components observed are given in **Table 4** along with the respective intensities. When the two lifetimes are close, it is common to report the mean lifetime. The average lifetimes have been calculated from the first two components (using Eqn.) and are also given in the **Table 4.**

$$\tau_{av} = \frac{\tau_{1p} I_{1p} + \tau_{2p} I_{2p}}{I_{1p} + I_{2p}} \quad (6)$$

Table 4: Positron life time values with their intensity *(* 'p' is used as subscript to distinguish the positron lifetimes and intensities from photoluminescence lifetimes and intensities)*

Sample	τ_{1p} **(ps)**	I_{1p} **(%)**	τ_{2p} **(ps)**	I_{2p} **(%)**	τ_{av} **(ps)**
Ag_2MoO_4	195.0± 3.2	68.0±2.6	370.8±9.7	29.9±2.6	248.7
Eu- doped	265.8± 3.6	90.8±3.9	460.5±7.8	7.0±1.8	279.7

In the undoped Ag_2MoO_4, the lifetime of the first component is 195 ps and second component is 370 ps. Upon doping with Eu, both the lifetimes increase with decrease I_2. The increase in the lifetime is 70 ps in τ_1 and about 90 ps in τ_2. The intensity of the second component reduced from ~30% to 7%. The results show that the first component is from the positron annihilations in the bulk while the second component is from the positron annihilations from the particle surface or annihilations in the larger bulk imperfections or voids. In the Ag_2MoO_4 sample, a significant fraction of positrons escape to the surface showing that the material having less trapping inside or relatively less defects in the particles. Upon Eu doping, the fraction of positrons annihilating inside the particle increases which also manifests as less number of positrons reaching the surface. The enhanced positron annihilation from inside the particle is due to the cation vacancies created by Eu doping. The increase in the τ_1 of about 70 ps suggests the creation of large cation vacancies. The presence of negatively charged vacancies in europium as indicated by enhanced τ_{1p} might be responsible for higher current density in the cyclic voltametric measurements. The average lifetime also increased by about 30 ps. The increased τ_2 indicate that the size of the surface related defects also increased upon Eu doping. The surface related defects aid the adsorption of oxygen on the surface and the ORR process in these materials.

Conclusions:

Spinel β-Ag_2MoO_4 was synthesized at room temperature itself using a simple and rapid co-precipitation method. Emission spectrum of pure β-Ag_2MoO_4 displays two bands at 445 and 550 nm in blue and green region respectively. The peak at 445 nm was attributed to charge transfer transition within distorted MoO_4 tetrahedra whereas green emission peak at 550 nm was attributed to presence of defects. Lifetime spectroscopy and DFT based calculations qualitatively explains host emission of β-Ag_2MoO_4 in green region due to presence of structural defects. Ag_2MoO_4: Eu can be easily excited using 395 and 465 nm giving an intense red $^5D_0 \rightarrow {}^7F_2$ emission at 615 nm which is otherwise rarely seen because of forbidden character of 395/465 nm. This is an important finding because high efficiency and low power consuming red emitting phosphor requires it to be excitable under near UV (~395 nm) or blue light (~465 nm). On doping europium there exists significant amount of energy transfer from MoO_4^{2-} anionic complex to Eu^{3+}. It is interesting that average lifetime value of Ag_2MoO_4 in Ag_2MoO_4:Eu^{3+} doped sample (14 .59 μs) is smaller than undoped sample (27.26 μs) under similar condition of λ_{ex} and λ_{em}. DFT calculation also shows that coincidence of Eu^{3+} d-states with CB as well as strong contribution of Eu^{3+} d-states in the impurity levels present in the vicinity of the Fermi level, the host (β-Ag_2MoO_4) to dopant (Eu^{3+}) energy transfer is highly probable. This also leads to conclusion that energy transfer has indeed taken place from molybdate ion to europium in doped sample leading to reduction in its lifetime. In case of Ag_2MoO_4: Eu; Ω_2 value was found to be greater than Ω_4 indicating high covalency and low symmetry around europium ion which is also observed in emission spectrum where EDT dominate MDT. This is well in agreement with high asymmetry value of Eu^{3+} in Ag_2MoO_4. Low phonon energy and high purity of red emission ($^5D_0$-$^7F_2$) along with good quantum efficiency (46.2 %) highlighted the potential of a completely unexplored β-Ag_2MoO_4 as a promising phosphor material. We have also explored its usability as catalyst for ORR and interestingly we found that Eu doped silver molybdate is a better catalyst than undoped one and large number of vacancies and vacancy clusters created by charge and size mismatch of europium seem to be aiding the oxygen adsorption and the catalysis. The presence of large vacancy clusters has been confirmed by large positron lifetimes.

Acknowledgement:

The authors sincerely thank Mr. Pradeep Samui, Product Development Division, BARC for XRD measurements.

Refernces:

1. E.K. Fodjo, D.W. Li, N.P. Marius. T. Albert, *J. Mater. Chem. A*, 2013, **1**. 2558.
2. H. Sinaim, A. Phuruangrat, S. Thongtem and T. Thongtem, *Mater. Chem. Phys*., 2012, **132**, 358.
3. G. Nagaraju, G.T. Chandrappa, J. Livage, *Bull. Mater. Sci*., 2008, **31**, 367.
4. M. Feng, M. Zhang, J.M. Song, X.G. Li, S.H. Yu, *ACS nano*, 2011, **5**, 6726.

5. Y. Wang, Y. Liu, X. Lu, Z. Li, H. Zhang, X. Cui, Y. Zhang, F. Shi, Y. Deng, *Electrochem. Commun.* 2012, **20**, 171.
6. W. Liu, M. S. Ji and S. F. Chen*, J. Hazard. Mater*., 2011, **186**, 2001
7. K. Kuribayashi, H. Harigae, Y. Suzuki, Y. Uchida, *Energy Proc*. 2011, **22**, 114.
8. L. Cheng, Q. Shao, M. Shao, X. Wei, Z. Wu, *J. Phys. Chem. C*, 2009, **113**, 1764.
9. W. Gulbinski, T. Suszko, *Wear*, 2006, **261**,867.
10. D. Zhou, W.B. Li, L.X. Pang, J. Guo, Z.M. Qi, T. Shao, Z.X. Yue, X. Yao, *J. Am. Ceram. Soc*., 2014, **97**, 3597.
11. Er-Yong Liu, Wen-Zhen Wang, Yi-min Gao, Jun-Hong Jia, Tribol. Lett. 2012, **47**, 21.
12. A. F. Gouveia, J. C. Sczancoski, M. M. Ferrer, A. S. Lima, M. R. M. C. Santos, M. Siu Li, R. S. Santos, E. Longo, and L. S. Cavalcante, *Inorg. Chem*., 2014, **53**, 5589.
13. P. Jena, Santosh K. Gupta, V. Natarajan, O. Padmaraj, N. Satyanarayana, *Mater. Res. Bull*. 2015, **64**, 223.
14. P. Jena, Santosh K. Gupta, V. Natarajan, M. Sahu, N. Satyanarayana, *J. Lumin*., 2015, **158**, 203.
15. F. Cheng, Z. Xia, X. Jing, Z. Wang, *Phys. Chem. Chem. Phys*., 2015, **17**, 3689.
16. H. Deng, N. Xue, Z. Hei, M. He, T. Wang, N. Xie, and R. Yu, *Opt. Mater. Exp*., 2015, **5**, 490.
17. Qing-Feng Wang, Y. Liu, Y. Wang, W. Wang, Y. Wan, Gui-Gen Wang, Zhou-Guang Lu, *J. Alloy. Compd*., 2015, **625**, 355.
18. H. Deng, Z. Zhao, J. Wang, Z. Hei, M. Li, H.M. Noh, J.H. Jeong, R. Yu, *J. Solid State Chem*., 2015, **228**, 110.
19. W. L. Chan, Z. Liu, S. Lu, P. A. Tanner, K.L. Wong, *J. Mater. Chem. C*, 2015, **3**, 960.
20. P. Kumar, B.K. Gupta, *RSC Adv*., 2015, **5**, 24729.
21. J. Lin, Q. Wang, Y. Zhang, Y. Zhang, *Cryst. Eng. Comm*., 2013, **15**, 5668.
22. A. Beltran, L. Gracia, E. Longo, and Juan Andres, *J. Phys. Chem. C* 2014, **118**, 3724.
23. S.A. Suthanthiraraj, Y.D. Premchand, *Ionics*, 2004, **10**, 254.
24. F. Rocca, A. Kuzmin, P. Mustarelli, C. Tomasi, A. Magistris, *Solid State Ionics*, 1999, **121**, 189.
25. S. Brown, A. Marshall, P. Hirst, P. *Mater. Sci. Eng., A* 1993, **173**, 23.
26. X. Cui, S.H. Yu, L. LI, L. Biao, H. Li, M. Mo, M.X. Liu, *Chem. Eur. J*, 2004, **10**, 218.

27. D.P. Singh, B. Sirota, S. Talpatra, P. Kohli, C. Rebholz, *J. Nanopart. Res*., 2012, **14**, 781
28. S.K. Gupta, P.S. Ghosh. N. Pathak, R. Tewari, *RSC Adv*., 2015, **5**, 56526.
29. S. K. Gupta, M. Sahu, K. Krishnan, M. Saxena, V. Natarajan and S.V. Godbole, *J. Mater. Chem. C, 2013,* **1,** 7054.
30. S.K. Gupta, M. Mohapatra, S.V. Godbole, V. Natarajan, *RSC Adv*. 2013, **3**, 20046.
31. S.K. Gupta, B. Rajeshwari, S.N. Achary, S.J. Patwe, A.K. Tyagi, V. Natarajan, R.M,. Kadam. *Eur. J. Inorg. Chem*, 2015, **2015**, 4429.
32. R. Shukla, S. K. Gupta, V. Grover, V. Natarajan, A.K. Tyagi, *Dalton Trans.* 2015, **44**,10628.
33. R. Phatak, S. K. Gupta, K. Krishnan, S.K. Sali, S.V. Godbole, A. Das , *Dalton Trans*. 2014*,* **43**, 3306
34. G. Kresse, J. Furthmueller, *Phys. Rev. B* 1996, **5**, 11169.
35. G. Kresse, J. Furthmueller, *Comput. Mater. Sci.* 1996, **6**, 15.
36. J. P. Perdew, K. Burke, M. Enzerhof, *Phys. Rev. Lett.* 1996, 77, 3685.
37. P. E. Blöchl, *Phys. Rev. B* 1994, **50**, 17953.
38. A.K. Arora, R. Nithya, S. Misra, T. Yagi, *J. Solid State Chem*., 2012, **196**, 391.
39. H. J. Monkhorst, J. D. Pack, *Phys. Rev. B* 1979, **13**, 5188.
40. http://www.ill.eu/sites/fullprof/
41. P. E. Blöchel, O. Jepsen, O. K. Andesen, *Phys. Rev. B*, 1994, **4**, 16223.
42. Y.V.B.D. Santana, J.E.C. Gomes, L. Matos, G.H. Cruvinel, A. Perrin, C. Perrin, J. Andres, J.A. Varela, E. Longo, *Nanomater. Nanotech*. 2014, **4**, 1.
43. S.K. Gupta, P.S. Ghosh, N. Pathak, A. Arya, V. Natarajan, *RSC Adv.,* 2014, **4**, 29202
44. M. Keskar, S. K. Gupta, R. Phatak, S. Kannan, V. Natarajan, *J. Photochem. Photobiol. A***,** 2015**,311**, 59.
45. C.R. Ronda, Luminescence: from Theory to Applications; Wiley- VCH: Weinheim, Germany, 2008
46. D. Yue, Q. Li, W. Lu, Q. Wang, M. Wang, C. Li, L. Jin, Y. Shi, Z. Wang, J. Hao, *J. Mater. Chem. C*, 2015, **3**, 2865.
47. S.K. Gupta, V. Grover, R. Shukla, K. Srinivasu, V. Natarajan, A.K. Tyagi, *Chem. Eng. J*, 2016, **283**, 126.
48. G. Blasse, *Phys. Lett. A*, 1968, **28**, 444.
49. A.K. Parchur, A.I. Prasad, S.B. Rai, R.S. Ningthoujam, *Dalton Trans*., 2012, **41**, 13810.

50. S. K. Gupta, P.S. Ghosh, M. Sahu, K. Bhattacharyya, R. Tewari, V. Natarajan, *RSC Adv.,* 2015, **5**, 58832.
51. S. Wang, E. Iyyamperumal, A. Roy, Y. Xue, D. Yu and L. Dai, *Angew. Chem. Int. Ed.*, 2011, **50**, 11756.
52. K. Gong, F. Du, Z.H. Xia, M. Durstock, L. Dai, *Science*, 2009,**323**,760.
53. F.H.B. Lima, J.F.R. de Castro, E.A. Ticianelli, *J. Power Sources*, 2006, **161**, 806.
54. X. Liu, K. Zhou, L. Wang, B. Wang, Y. Li, *J. Am. Chem. Soc*., 2009, **131**, 3140.

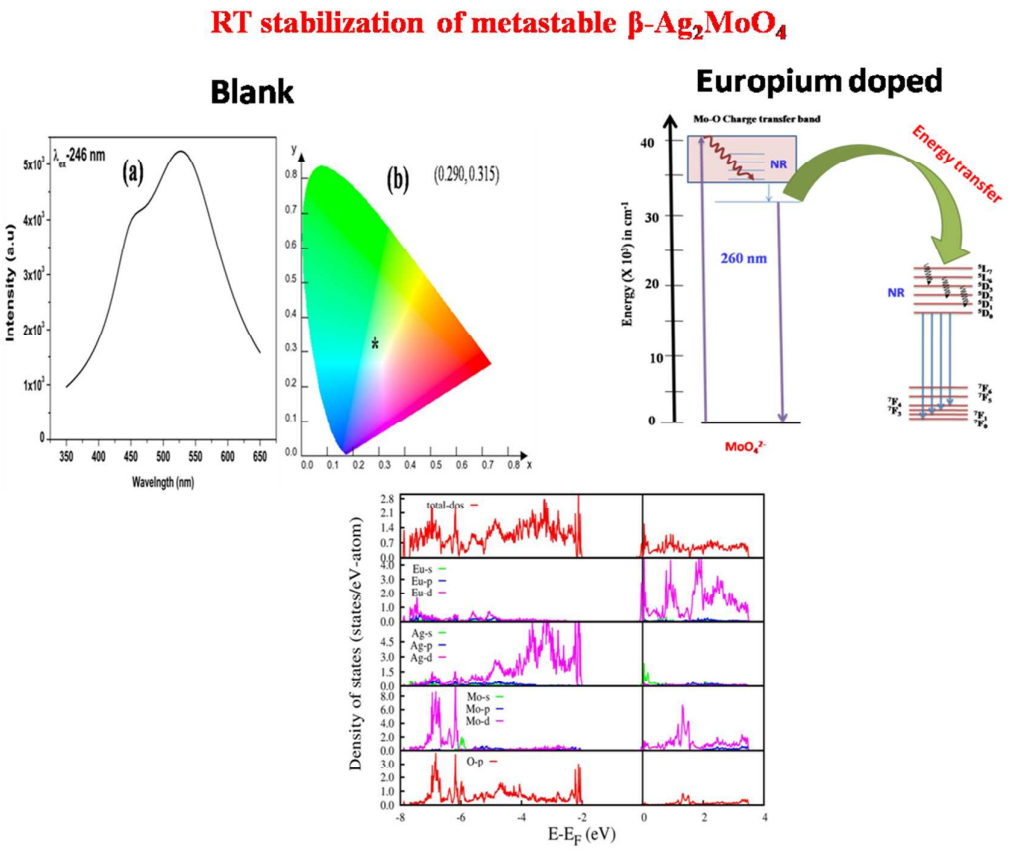

Pure and Europium doped β-Ag_2MoO_4 is explored for photoluminescence and electrocatalytic properties. Host dopant energy transfer process is explained theoretically.